Thermodynamic anomaly above the superconducting critical temperature in the quasi-one-dimensional superconductor $Ta_4Pd_3Te_{16}$

T. Helm,[1,2,*] F. Flicker,[1] R. Kealhofer,[1] P. J. W. Moll,[1,2] I. M. Hayes,[1,2] N. P. Breznay,[1,2] Z. Li,[1] S. G. Louie,[1] Q. R. Zhang,[3] L. Balicas,[3] J. E. Moore,[1,2] and J. G. Analytis[1,2]

[1]*Department of Physics, University of California, Berkeley, California 94720, USA*

[2]*Materials Science Division, Lawrence Berkeley National Laboratory, Berkeley, California 94720, USA*

[3]*National High Magnetic Field Laboratory, Florida State University, Tallahassee, Florida 32310, USA*

(Received 5 July 2016; revised manuscript received 21 January 2017; published 13 February 2017)

We study the intrinsic electronic anisotropy and fermiology of the quasi-one-dimensional superconductor $Ta_4Pd_3Te_{16}$. Below $T^* = 20$ K, we detect a thermodynamic phase transition that predominantly affects the conductivity perpendicular to the quasi-one-dimensional chains. The transition relates to the presence of charge order that precedes superconductivity. Remarkably, the Fermi surface pockets detected by de Haas–van Alphen oscillations are unaffected by this transition, suggesting that the ordered state does not break any translational symmetries but rather alters the scattering of the quasiparticles themselves.

DOI: 10.1103/PhysRevB.95.075121

I. INTRODUCTION

Superconducting materials with extreme anisotropies in their electronic normal-state behavior are of immense interest for studying the relationship between dimensionality, broken symmetry, and unconventional mechanisms of superconductivity. For example, both cuprate and iron-pnictide superconductors are proximal to magnetic and possibly "nematic" orders. In the case of the cuprates, the recent discovery of charge density order has ignited debate as to whether such thermodynamic phases are competing, causal, or benignly coincident with superconductivity [1–3]. This ground-state electronic competition is particularly important in quasi-one-dimensional (Q1D) systems [4,5], which generically show charge order and often also exhibit unconventional superconductivity. Recently, the Q1D ternary superconductor $Ta_4Pd_3Te_{16}$ (TPT) has been suggested to be proximal to quantum ordered states and a possible host for unconventional superconductivity [6–8].

TPT is a layered material with a monoclinic crystal structure [9]. The high-conductivity direction coincides with the b axis, parallel to the $PdTe_2$ chains lying within flat layers separated by $TaTe_3$ chains and Ta_2Te_4 double chains [see Fig. 1(a)]. Well-studied Q1D systems such as the organic tetramethyltetraselenafulvalene (TMTSF)-PF_6 [10] or purple bronze $Li_{0.9}Mo_6O_{17}$ [11] possess complex phase diagrams with evidence of spin or charge density wave instabilities [5]. However, despite several recent studies, TPT has not shown unambiguous evidence of an instability competing with its superconducting phase. This may be because TPT is significantly more isotropic: although direct resistivity measurements have been unavailable until now, measurements of the upper critical field have given indirect evidence that the electronic anisotropy in this compound is relatively weak [6,7]. Recent density functional theory (DFT) calculations predict that the system is multiband in nature [12], showing a combination of Q2D, 3D, and several Q1D bands at the Fermi level E_F that could account for earlier evidence of unconventional behavior in the thermal conductivity and heat capacity [6,7]. Aside from superconductivity, no other bulk properties show clear thermodynamic evidence for an additional order parameter, raising the possibility that there may not be any other broken symmetry proximal to superconductivity. It is therefore important to determine the underlying Fermi surface as well as the intrinsic electronic anisotropy in order to understand the apparent absence of other ordered states in the case of TPT.

In this work, we report the existence of a thermodynamic transition above the superconducting critical temperature (T_c), indicative of a nearby phase instability in TPT. By applying torque magnetometry and magnetotransport, we observe de Haas–van Alphen (dHvA) oscillations that confirm the multiband nature of TPT's bulk Fermi surface. Using focused ion beam (FIB) microstructuring, we fabricated devices enabling measurements of the resistivity along the interchain (a^*) and interlayer (c) directions [see Fig. 1(a)]. Remarkably, the anomaly is only pronounced in the transport channel perpendicular to the chains, setting in at $T^* = 20$ K, but is quite subtle in all other directions. Finally, there is no change in the dHvA frequency observed across T^*, suggesting that the Fermi surface experiences no reconstruction at this temperature. We discuss possible explanations for the observed anomaly and its relationship to superconductivity, and in particular whether T^* marks the onset of charge density wave (CDW) fluctuations or a thermodynamic phase transition corresponding to an incommensurate-to-commensurate CDW lattice lock-in.

II. EXPERIMENTAL AND CALCULATIONAL METHODS

Single crystals of TPT were grown using a self-flux with excess tellurium at temperatures as high as 1000 °C, similar to the method reported by Jiao *et al.* [7]. High-resolution single-crystal x-ray diffraction was performed at the Advanced Light Source (ALS) at Lawrence Berkeley National Laboratory that confirmed the quality of the crystals and their orientation. Hence, contributions from impurity phases to the magnetic quantum oscillation data presented in the following can be ruled out.

*Present address: Max Planck Institute for Chemical Physics of Solids, 01187 Dresden, Germany; toni.helm@cpfs.mpg.de

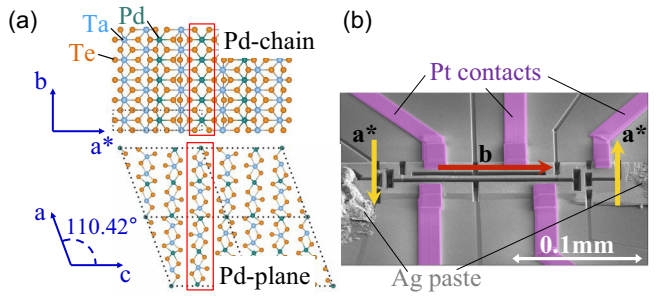

FIG. 1. (a) Crystal structure of TPT with the conventional unit cell (dotted) in the representation C2/m. (b) Scanning electron microscope image of a transport device prepared by FIB etching. Red and yellow arrows highlight the b and a^* directions, respectively.

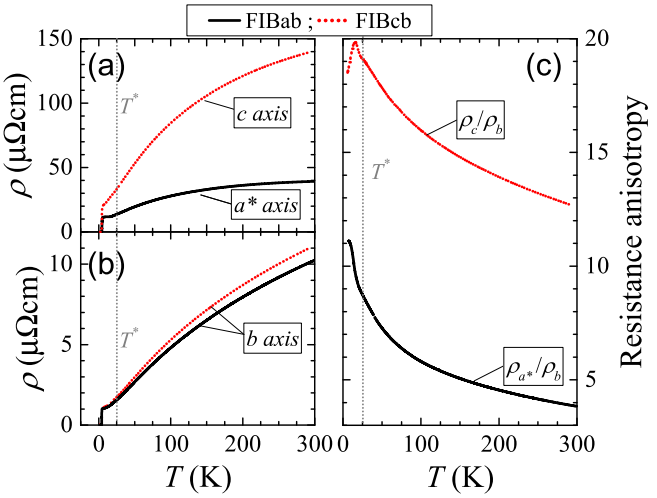

FIG. 2. (a),(b) Resistivity along the a^* and b axes for device FIBab and along the b and c axes for device FIBcb plotted against temperature; the gray dotted line highlights the anomaly at T^*. (c) Resistivity anisotropy ρ_i/ρ_b for each device, with $i = a^*,c$.

Electrical transport devices were prepared by FIB etching and *in situ* deposition of platinum or gold contacts onto thin flakes of TPT, cleaved from the as-grown needlelike crystals. Sample sizes were a few micrometers in thickness and a couple of hundred micrometers in length. Low-ohmic contacts with contact resistances of the order of 1Ω were achieved. A device that has been microstructured to measure b-axis and a^*-axis conductivity is shown in Fig. 1(b).

Magnetic torque and magnetotransport experiments were performed in fields up to 45 T at the National High-Magnetic Field Laboratory (NHMFL). Both piezoresistive microcantilevers from Seiko and capacitive cantilevers built by NHMFL were used as torque magnetometers. Further torque and magnetotransport measurements were performed in a Cryogenic Ltd. 16 T cryogen-free magnet system.

Fully relativistic first-principles calculations were performed using density functional theory (DFT) under the local density approximation (LDA) [13] and implemented using the QUANTUM ESPRESSO software [14]. Starting from the experimental crystal lattice parameters, all internal atomic positions were allowed to relax until interatomic forces were less than 5 meV/Å. High-resolution Fermi surface data were obtained by non-self-consistent calculations on a $50 \times 50 \times 30$ k-point grid in the first Brillouin zone and were plotted using XCRYSDEN [15]. The dHvA simulation curves were calculated using the Supercell K-space Extremal Area Finder (SKEAF) code [16].

III. MAGNETOTRANSPORT AND MAGNETIC SUSCEPTIBILITY

Figures 2(a) and 2(b) show the resistivity, measured with an applied current along the three crystallographic directions, as a direct measure of the transport anisotropy. We microstructured two devices: one made to measure the a^* and b directions simultaneously, denoted FIBab [shown in Fig. 1(b)], and the other measuring the b and c crystallographic directions simultaneously, denoted FIBcb. Note that FIBab and FIBcb, which are cut from crystals belonging to the same batch, have highly reproducible b-axis resistivity ρ_b, indicating homogeneity within the batch. The resistivity anisotropy grows monotonically as the temperature is lowered: at room temperature, the resistivity ratios $(\rho_{a^*} : \rho_b : \rho_c) \sim 4 : 1 : 13$, while at low temperature (just above $T_c = 4.6$ K), $(\rho_{a^*} : \rho_b : \rho_c) \sim 10 : 1 : 20$, as shown in Fig. 2(c). Due to possible mixing between different conduction channels, these ratios are lower bounds of the intrinsic resistivity anisotropies. Evidently, the system becomes much more conductive along the b axis than along any other axis, suggesting that scattering becomes significantly suppressed along the chains. We find that the temperature dependence of both ρ_c/ρ_b and ρ_{a^*}/ρ_b shows shallow kinks at $T^* = 20$ K, followed by peaks above T_c.

As can be seen in Fig. 3(a), which shows the resistivity normalized to the 6 K value for all three channels, this peak is related to a resistivity anomaly which is most pronounced in ρ_{a^*}. In contrast, the data for ρ_b and ρ_c show very weak features in this region. On taking the derivative $d\rho_i/dT$ $[i \in (a^*,b,c)]$, shown in Fig. 3, we see that all crystallographic directions exhibit an anomaly within a few Kelvin of T^*. The gray shaded area in Fig. 3 highlights the temperature range $T = 8$–20 K, within which we observe deviations from normal-metallic behavior. For the a^* direction, we find a clear minimum at 14 K, but a broad onset starting slightly above T^*. Along the b direction, we find a weak change in slope accompanied by a peak slightly below T^*. Similarly, a peak develops for $d\rho_c/dT$ below T^* with its maximum at 14 K. Given that the conductivity along b is over ten times greater than that along a^* at these temperatures [see Fig. 2(c)], it seems unlikely that this feature is exclusively due to mixing of ρ_b with ρ_{a^*}; rather, it is intrinsic, albeit weak enough to have been overlooked in previous measurements. We find that the T^* anomaly is independent of the substrate (either sapphire or silicon), sample thickness (ranging from 15 to 1 μm), and attachment method (either glue or van der Waals attraction). We can therefore rule out any substrate strain effects as a cause of the observed features.

The derivatives $d\rho_b/dT$ and $d\rho_c/dT$ are strongly linear at $T < T^*$, consistent with the onset of $\rho \propto T^2$ Fermi liquid-like behavior, which may be a precursor to the onset of superconductivity at $T_c \sim 4$ K. Interestingly, the temperature at which the anomaly occurs is weakly sensitive to the application

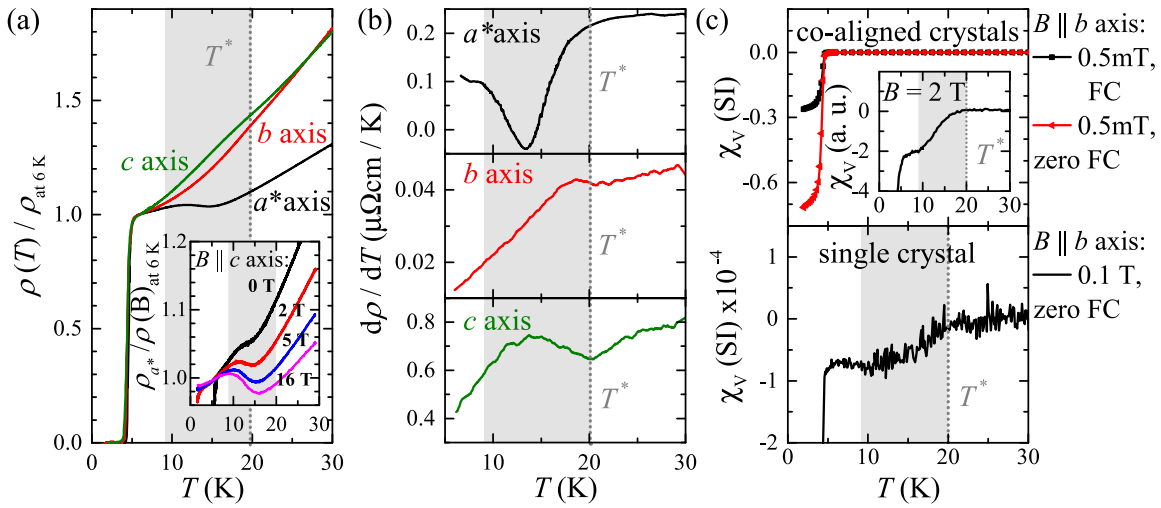

FIG. 3. (a) Resistivity (normalized by its value at $T = 6$ K) along all three crystal axes (a^*, b, and c) plotted against temperature; the gray dotted vertical line marks T^* (see text). Inset: temperature dependence of the a^* resistivity in a constant magnetic field up to 16 T applied parallel to c. (b) Derivatives of the resistivity, $d\rho_i/dT$, for each transport direction, with $i = a^*,b,c$. (c) Temperature dependence of the magnetic susceptibility χ_v for a small number of TPT coaligned single crystals (upper panel) and a separated single crystal (lower panel), oriented with the b axis parallel to the applied magnetic field; insets show closeup of background-subtracted high-field data. Note that T^* marks the temperature below which both resistivity and magnetization show a clear feature indicative of a thermodynamic phase transition; the anomalous temperature region is highlighted by the gray shaded area.

of magnetic field [inset Fig. 3(a)], suggesting that it is strongly pinned electronically or that it is related to the softening of a phonon mode. However, the magnetoresistance is much larger below the anomaly than above, suggesting the carriers are significantly more mobile at $T < T^*$. A similar response is observed in the unconventional superconductor $BaFe_2As_2$, where a strong scattering channel is gapped out at the Néel transition, strongly enhancing the mobility of the itinerant carriers [17].

We studied the magnetic volume susceptibility χ_V of TPT around T^* for a few dozen coaligned single crystals with an average width of about 100 μm, thickness of 20 μm, and length of 3 mm, pointing with their b directions parallel to the field. In Fig. 3(c), we show zero-field-cooled and field-cooled data measured at a field of 100 mT exhibiting strong diamagnetism setting in at the superconducting critical temperature $T_c = 4.6$ K, with a transition width of about 1 K. The inset of Fig. 3(c) shows data recorded at a field of 2 T after subtracting off the background (related to the sample holder). Below 20 K, there is a broad anomaly, manifested as a reduction in the magnetic susceptibility. We also observed a similar decrease of χ_V for a separated single crystal [see the lower panel of Fig. 3(c)]. The presence of the anomaly was confirmed for three different polycrystalline samples and three single crystals in three different superconducting quantum interference device (SQUID) magnetometers independently, ruling out contributions from sample holders and magnetic contamination of the sample chambers.

In the simplest model, the strong reduction above the superconducting transition can be attributed to a decrease in the electronic density of states or, equivalently, a decrease in the electronic effective mass (note that this is consistent with the enhanced mobility we observe). The consistency between transport and susceptibility data is strong evidence that the T^* anomaly is a true thermodynamic transition, indicative of a substantial change in the electronic properties of the system.

IV. MAGNETIC QUANTUM OSCILLATIONS AND DFT BAND STRUCTURE

In order to better understand the low-temperature ground state, we study the Fermi surface by measuring magnetic quantum oscillations in high-purity crystals. Background-subtracted de Haas–van Alphen (dHvA) oscillations, recorded in a dc magnetic field at $T = 1.5$ K, are shown in Fig. 4(a). Multiple frequencies superimposed on a quadratic-in-field magnetic background torque τ_{bg} are observed. Fast Fourier transforms (FFTs) of the data for each angle θ ($\theta = 0$ defined to have the applied magnetic field, $\mathbf{B}$, parallel to the c axis) as shown in Fig. 4(b) for $\theta = 57^\circ$, provide access to the angle dependence of the various frequencies. In Fig. 4(c), we show the angle dependence of the major frequency peaks for two separate experiments: in low fields, where $B < 16$ T (green diamonds), and in fields between 25–45 T (black circles). In the high-field data, at least three distinct frequencies are discernible, labeled F_1, F_2, and F_3. However, only F_1 and F_2 were discernible in fields below 16 T. We therefore screened three different growth batches and only observed contributions from F_1 and F_2.

As the field orientation is tilted away from $\mathbf{B}||c$, the smallest frequency F_1 stays relatively unaffected, indicative of a three-dimensional (3D) Fermi surface. At 30 T, the oscillation period for a frequency of about 100 T can be estimated to $\approx$9 T precision. Therefore, for a field window of 25–45 T, at most four maxima can be observed, reducing the reliability of FFT analysis for such low frequencies. By contrast, F_2 and F_3 trace a trajectory that tracks the perpendicular component of field

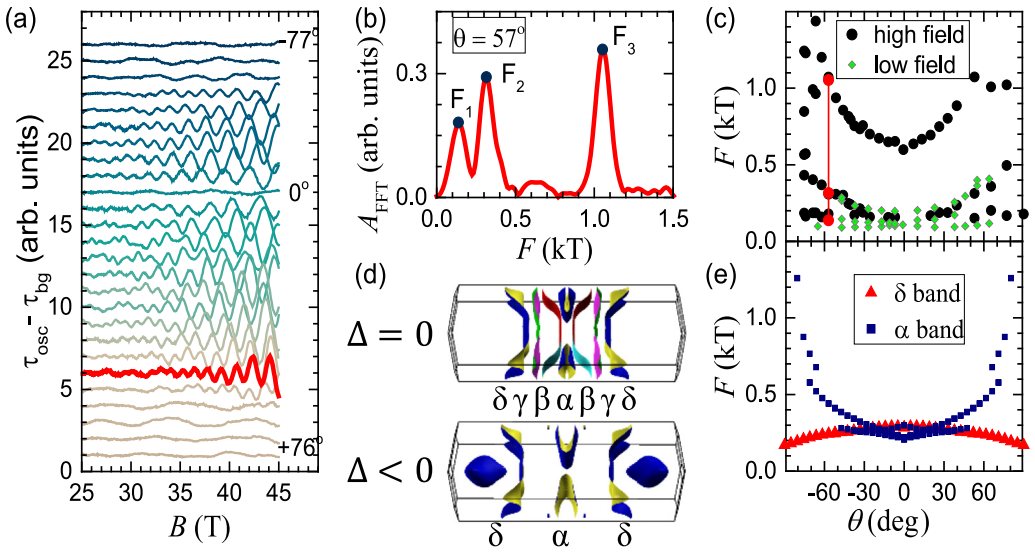

FIG. 4. (a) Background-subtracted dHvA oscillation data for various field orientations recorded at $T = 1.5$ K in the 45 T hybrid magnet. $\theta = 0^\circ$ corresponds to the applied field along the c axis. (b),(c) Frequency values obtained from fast Fourier transform (FFT) of the data in (a). The field ranges from 25–45 T (black spheres) and 5.5–16 T (green diamonds). (d) Fermi surfaces for unshifted and shifted chemical potential with $\Delta = 0$ and -27 meV, respectively. (e) DFT-calculated dHvA oscillation frequencies originating from the α and δ bands of the Fermi surfaces shown in (d).

$1/B\cos\theta$, indicative of a quasi-two-dimensional (Q2D) Fermi surface pocket. F_3 was only clearly visible in the high magnetic field data; it appeared close to the background noise level for the lowest temperatures in the experiments below 16 T. We reproduced the oscillation spectra for various samples by application of two distinct measurement techniques: capacitive and piezoresistive torque magnetometry. The clear presence of Q2D and 3D Fermi surface components can explain the relatively weak anisotropic character of TPT's transport behavior compared to other Q1D materials.

TPT's Fermi surface predicted by DFT calculations is shown in Fig. 4(d). It consists of four distinct bands: a cylindrical α band centered around the X point, and three Q1D bands labeled β, γ, and δ, respectively. The δ band shows a strong effect on the position of the chemical potential Δ. By only minor changes in Δ, equivalent to doping holes, this Fermi surface sheet acquires a more complex appearance, exhibiting a three-dimensional extension along the k_y direction in the Brillouin zone.

In Fig. 4(e), we show for comparison the results of DFT calculations for the Fermi surface at zero temperature. With a shift of the chemical potential by $\Delta \approx 27$ meV, our calculations broadly agree with low-frequency oscillations originating from the cylindrical α and the 3D part of the δ band. However, the higher-frequency oscillation F_3 cannot be simultaneously recovered, suggesting that the predicted band structure does not adequately capture the low-temperature ground state. This discrepancy could be evidence for band reconstruction due to density-wave-broken translational symmetry. An additional frequency that only shows up in high magnetic fields could arise from the magnetic breakdown effect and cannot be ruled out as an origin of F_3.

To investigate whether the Fermi surface is affected by the T^* anomaly, we track the dHvA signal to higher temperatures (Fig. 5, lower panels). We are able to resolve clear quantum oscillations in low fields below 16 T. The dHvA oscillation data are presented in Fig. 5(a). Though the higher frequency is quickly suppressed with temperature, the 3D pocket at $\sim$100 T can be tracked to 25 K [Fig. 5(b)]. We observe no significant changes for this frequency in the FFT spectrum, suggesting that little or no bandfolding occurs at $T^* = 20$ K. While it is possible that this pocket exists at a point in the Brillouin zone that is not reconstructed, this would be difficult to reconcile with our DFT calculations. One scenario, which we discuss below, is that T^* marks an incommensurate-commensurate charge density wave lock-in transition, which requires no additional translational symmetry breaking.

The effective masses of each of the Fermi surface sheets are extracted from fits of the temperature-dependent oscillation amplitude at a constant field orientation to the Lifshitz-Kosevich temperature damping factor $R_T = K\mu T/B \sinh(K\mu T/B)$, with $K = -14.694$ T/K [18]. We find $\mu_{F_1} \approx (0.14 \pm 0.02)m_e$ and $\mu_{F_2} \approx (0.2 \pm 0.03)m_e$, with m_e the bare electron mass. The fits are shown in Fig. 5(c). The measured and calculated masses are quite similar, suggesting that correlation effects only weakly renormalize the electronic system. The difference between the two values supports the idea that the two Fermi surface sheets are located on different bands.

V. DISCUSSION

Owing to the Q1D nature of TPT, it has long been speculated that a Peierls instability to charge density wave (CDW) formation may be present [6,7,12]. The best evidence for such a state comes from scanning tunneling microscopy (STM) measurements on the surface of the material, which see a clear modulation of period four in the along-chain b direction at 4 K, in one of the three chain types [19]. Analyzing the Fourier transform of the STM data, harmonic multiples of the CDW satellite peaks can be seen to derive from the same chains, suggesting a modulation of the sinusoidal pattern

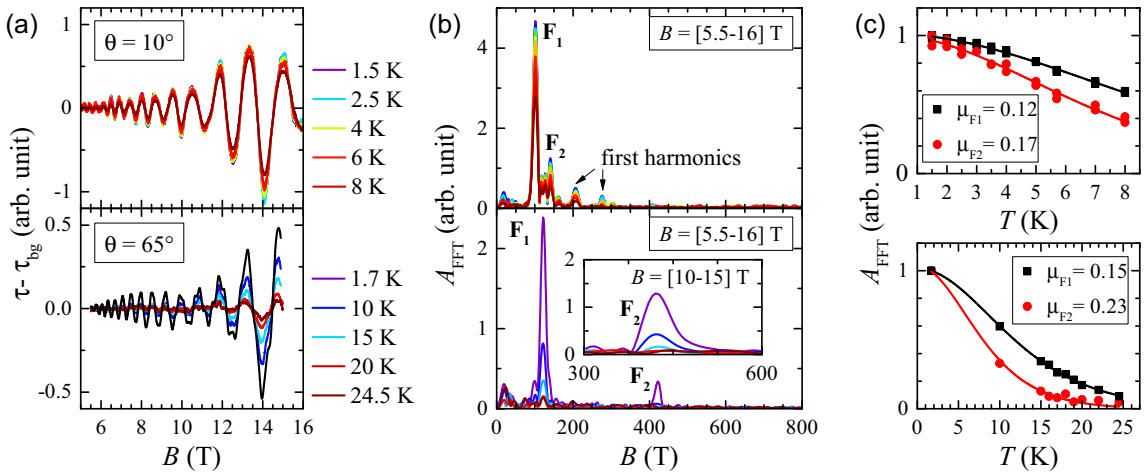

FIG. 5. (a) Background-subtracted de Haas–van Alphen oscillations measured with a piezoresistive torque magnetometer in a dc 16 T magnet for various temperatures, with $\theta = 10^\circ$ in the upper panel and $\theta = 65^\circ$ in the lower. (b) FFT of the data shown in (a) over a field window of 5.5–15 T. The inset shows FFT data for B = 10–15 T. (c) Effective mass plots. Solid lines are fits according to Lifshitz-Kosevich theory (see main text).

consistent with a commensurate period-four CDW. From our DFT calculations, we see that the Q1D γ bands are nested with separation $\approx 0.27b^*$, consistent with a Peierls instability developing from these bands, making it likely to be the Q1D chains developing CDW order.

Despite this observation of a CDW at 4 K, no studies have so far observed evidence of a thermodynamic phase transition corresponding to the ordering event. The arrival of a commensurate CDW upon cooling a low-dimensional system would normally be preceded by two events: in decreasing temperature, we would first expect the onset of a fluctuating, short-range-correlated CDW regime [20–23]; then, second, the development of an incommensurate CDW state, eventually locking into the commensurate state at a lower temperature [24–26]. The thermodynamic transition we see at 20 K is unlikely to be the development of true charge order along the b direction, as this would be accompanied by a significant boost in the along-chain resistivity and a more pronounced specific-heat discontinuity. We instead consider the possibility that the observed transition is related to either the onset of fluctuations, akin to what is seen in other unconventional superconductors such as the cuprates [27,28], or an incommensurate-to-commensurate lock-in transition.

The low effective dimensionality of TPT suggests its CDW transition will be preceded by significant fluctuations over a range of temperatures [22,23]. The absence of evidence of CDW order in bulk probes of TPT—resistivity, heat capacity, thermal conductivity [6,7,29], and arguably Raman spectroscopy [30]—as well as our quantum oscillation measurements showing no Fermi surface reconstruction between 300 and 1.5 K, suggest that the CDW seen by STM at 4 K could be stabilized by the surface, corresponding in the bulk to the fluctuating regime rather than true CDW order. The transition we see at 20 K could be the turning on of these fluctuations. A sharp turn on of CDW fluctuations has previously been proposed to account for a resistivity bump in the Q2D transition-metal oxide bronze $P_4W_{10}O_{38}$ [31,32] and has been predicted in the Q2D transition-metal dichalcogenide $NbSe_2$ [23,33]. Despite the fluctuating CDW order being along the b-direction chains, it would not necessarily give a strong resistivity boost in this direction. The three-dimensional character of the fluctuations could plausibly induce an interchain resistivity bump as instantaneous regions of CDW attempt to order the charge on the neighboring chains, as seen in other Q1D systems on approach to spin or charge density wave transitions [10,34,35].

Among CDW materials, the Q2D rare-earth tritellurides RTe_3 (R = lanthanide) have particularly similar structures to that of TPT, featuring three independent chains making up planes [36,37]. A CDW forms in the along-chain direction across the family. While the CDW formation is accompanied by a boost to along-chain resistivity, a larger resistivity boost is seen in the in-plane interchain direction, much as we are seeing in TPT (Fig. 4) [37]. In RTe_3, this can be accounted for by a simple one-electron model of conductivity, factoring in Fermi surface reconstruction by the CDW [37]. We reproduced this calculation at zero temperature for TPT using our DFT band structure, taking account of fluctuating CDW order simply by removing the γ bands (expected to give a gross overestimate of the effect). With all bands in place, we find resistivity anisotropies of $\rho_{a^*} : \rho_b : \rho_c = 116 : 1 : 165$, compared to our measured values of around $10 : 1 : 20$. Removing the γ bands, we find $\rho^{(\alpha+\beta+\gamma+\delta)}/\rho^{(\alpha+\beta+\delta)} = \{1.6, 2.4, 1.3\}$, i.e., the biggest resistivity boost in the along-chain direction. We varied the chemical potential over a range of 0.1 meV and found no qualitative change. The results demonstrate that if the 20 K resistivity anomaly is due to the onset of CDW fluctuations, this simple one-electron model cannot account for the result. This could either be a failing of the model or could suggest the importance of correlated electron effects. Despite the structural similarity of the RTe_3 compounds to TPT, the RTe_3 family has a peculiarity in its Fermi surface topology better suiting it to such an interchain resistivity enhancement [38]. A further challenge for this hypothesis is to explain why the fluctuations turn on at such a low temperature, although this

could potentially be accounted for by the fact that TPT is not especially one dimensional in character.

The consistency between transport and susceptibility data suggests that the 20 K anomaly is a true thermodynamic phase transition. Motivated by this fact, we consider a second scenario in which the resistivity bump is due to an incommensurate-to-commensurate lock-in transition. Commensurate CDW (CCDW) systems are generically expected to develop via the evolution of the wave vector of an incommensurate CDW (ICDW) taking advantage of lattice lock-in energy at lower temperatures [24,39]. The evolution is continuous over a range of temperatures before jumping discontinuously at the transition, as seen for example in (Q2D) $2H$-$TaSe_2$ ($T_{\mathrm{ICDW}} = 122.3$ K, $T_{\mathrm{CCDW}} = 92$ K) and (Q1D) tetrathiafulvalene-tetracyanoquinodimethane (TTF-TCNQ) ($T_{\mathrm{ICDW}} = 54$ K, $T_{\mathrm{CCDW}} = 38$ K) [25,32,36,40]. This proposal naturally accounts for the discrepancy between the quantum oscillation data with DFT, as well as the lack of Fermi surface reconstruction at 20 K, since the band structure is *already* reconstructed at higher temperatures by the ICDW. No significant change occurs in ρ_b at the commensurate-to-incommensurate transition as the gap remains largely unchanged, but the bump in ρ_{a^*} can be accounted for by the alignment of the CDWs in the interchain direction when they are required to lock into the monoclinic lattice. The question then arises as to at what temperature the ICDW itself develops. We see no evidence of this phase transition up to 300 K. Such a difference in commensurate and incommensurate transition temperatures is large but not unprecedented, with (Q2D) $2H$-TaS_2 exhibiting $T_{\mathrm{ICDW}} = 543$ K and $T_{\mathrm{CCDW}} = 183$ K [36]. Indeed, Raman scattering in TPT may see some indication of CDW order at temperatures as high as 150 K [30]. It should be noted that in this scenario, the agreement between the dHvA spectrum and DFT calculations of the Fermi surface would be coincidental rather than comprehensive.

The two scenarios, CDW fluctuation onset and a lock-in transition, could be distinguished and verified by high-resolution x-ray scattering. The incommensurate-to-commensurate transition scenario could also be tested by nonlinear conductivity measurements, since an ICDW is expected to have a lower electric field threshold to depinning [41]. So far we have not observed any deviations that might hint towards an enhancement in conductivity due to a sliding CDW. In both scenarios, the precise details of the interchain coupling induced by Coulomb repulsion between neighboring CDWs remain to be elucidated.

Recently, a study of nuclear magnetic and nuclear quadrupole resonance (NMR and NQR) in TPT has shown further experimental evidence for an event below $T = 20$ K [42]. A peak in the temperature dependence of the spin-lattice relaxation rate and a broadening of the linewidth data indicate a thermodynamic phase transition. However, the absence of clear lines in the NMR spectrum at temperatures below 20 K, expected for a static long-range order [43], speaks against a full CDW ordering transition at T^*. This would agree with our observations of no discernible band folding at $T^* = 20$ K and a very weak effect of this event on the electrical transport along the chains. The observed strong feature for current applied along the a^* direction, correlating with a feature observed in the magnetic susceptibility, plus the significant enhancement of the anisotropy as temperature is decreased, support our proposed scenarios.

The origin of the observed enhancement of the resistance anisotropy is not clear. This behavior strongly resembles a nematic response analogous to that seen in Fe-based superconductors [44]. Other mechanisms, including anisotropic scattering, or structural changes with temperature cannot be ruled out at this point. High-resolution, low-temperature x-ray scattering could provide insight into the influence of temperature on the lattice parameters and high-resolution scanning tunneling spectroscopy could reveal whether there are temperature-dependent changes to the density of states or scattering mechanisms.

The question remains as to whether the phase transition at $T^* \approx 20$ K has a direct effect on the development of superconductivity at 4.6 K. This would seem unlikely given the large separation of the two energy scales. We do, however, note that approaching T^* from above, the transition corresponds to the cessation of growth of the transport anisotropy [see Fig. 2(b)] and the simultaneous development of apparent Fermi liquid-like behavior, evidenced by a T^2 resistivity dependence [see Fig. 3(b)]. The transition may therefore be indirectly responsible for the superconductivity by establishing a Fermi liquid at low temperature which is then unstable to the formation of Cooper pairs by a standard BCS-type mechanism.

VI. CONCLUSIONS

In this work, we have measured the magnetization and transport properties of the low-dimensional superconductor TPT. By utilizing focused ion beam microstructuring, we have revealed the intrinsic transport anisotropy of this material which grows precipitously as the temperature is lowered. At $T^* = 20$ K, the transport shows a clear anomaly that is especially pronounced in the a-axis conductivity. With careful measurements, this anomaly also has a (more subtle) signature in the magnetization and in the transport along other crystallographic directions, which is perhaps why it was missed in previous measurements. This subtle nature of the transition is likely intrinsic, and our de Haas–van Alphen studies hint as to why this might be so. Specifically, we show that a 3D Fermi surface shows no sign of reconstruction above T^*, suggesting that there is no translational symmetry breaking across this transition. We suggest two scenarios as to how this could come about: a lock-in transition or the onset of strong CDW fluctuations, but further measurements are required to decide between the two. Finally, it seems unlikely that the mechanism behind the T^* anomaly drives superconductivity. Our data show that the T^* transition appears to make the system more Fermi-liquid-like, as well as ending the precipitous growth of the transport anisotropy observed above T^*, thus setting the scene for the superconducting condensate to form.

ACKNOWLEDGMENTS

We would like to acknowledge the extremely helpful and efficient collaboration of S. J. Teat and K. J. Gagnon for characterizing and orienting the single crystals at beam line 11.3.1 of the Advanced Light Source (ALS) in Lawrence Berkeley National Laboratory in preparation of the individual

experiments. We are grateful for the help of A. Frano in terms of performing measurements of the magnetic susceptibility in a Quantum Design SQUID magnetometer in the laboratory of R. J. Birgeneau. We thank K. R. Shirer and M. Baenitz for stimulating discussions. The ALS is supported by the Director, Office of Science, Office of Basic Energy Sciences (BES), of the U.S. Department of Energy (DOE) under Contract No. DE-AC02-05CH11231. T.H. was supported by the Quantum Materials FWP, U.S. DOE, BES, Materials Sciences and Engineering Division, under Contract No. DE-AC02-05CH11231. F.F. acknowledges financial support from a Lindemann Trust Fellowship of the English Speaking Union. L.B. is supported by the U.S. DOE, BES through Award No. DE-SC0002613.

[1] T. Wu, H. Mayaffre, S. Kramer, M. Horvartic, C. Berthier, W. N. Hardy, R. Liang, D. A. Bonn, and M.-H. Julien, Magnetic-field-induced charge-stripe order in the high-temperature superconductor $YBa_2Cu_3O_y$, Nature (London) **477**, 191 (2011).

[2] H. M. Christensen, H. Jacobsen, T. A. Maier, and B. M. Andersen, Magnetic Fluctuations in Pair-Density-Wave Superconductors, Phys. Rev. Lett. **116**, 167001 (2016).

[3] S. Badoux, W. Tabis, F. Lalibert, G. Grissonnanche, B. Vignolle, D. Vignolles, J. Bard, D. A. Bonn, W. N. Hardy, R. Liang, N. Doiron-Leyraud, L. Taillefer, and C. Proust, Change of carrier density at the pseudogap critical point of a cuprate superconductor, Nature (London) **531**, 210 (2016).

[4] R. Peierls, Zur Theorie der elektrischen und thermischen Leitfähigkeit von Metallen, Ann. Phys. **396**, 121 (1930).

[5] J.-P. Pouget, The Peierls instability and charge density wave in one-dimensional electronic conductors, C. R. Phys. **17**, 332 (2016).

[6] J. Pan, W. H. Jiao, X. C. Hong, Z. Zhang, L. P. He, P. L. Cai, J. Zhang, G. H. Cao, and S. Y. Li, Nodal superconductivity and superconducting dome in the layered superconductor $Ta_4Pd_3Te_{16}$, Phys. Rev. B **92**, 180505 (2015).

[7] W.-H. Jiao, Z.-T. Tang, Y.-L. Sun, Y. Liu, Q. Tao, C.-M. Feng, Y.-W. Zeng, Z.-A. Xu, and G.-H. Cao, Superconductivity in a layered $Ta_4Pd_3Te_{16}$ with $PdTe_2$ chains, J. Am. Chem. Soc. **136**, 1284 (2014).

[8] Z. Du, D. Fang, Z. Wang, Y. Li, G. Du, H. Yang, X. Zhu, and H.-H. Wen, Anisotropic superconducting gap and elongated vortices with Caroli–de Gennes–Matricon states in the new superconductor $Ta_4Pd_3Te_{16}$, Sci. Rep. **5**, 9408 (2015).

[9] A. Mar and J. A. Ibers, Synthesis, crystal structure and electrical conductivity of a new layered ternary telluride Ta_4 Pd_3 Te_{16}, J. Chem. Soc., Dalton Trans., 639 (1991).

[10] M. Dressel, Ordering phenomena in quasi-one-dimensional organic conductors, Naturwissenschaften **94**, 527 (2007).

[11] N. Wakeham, A. F. Bangura, X. Xu, J. F. Mercure, M. Greenblatt, and N. E. Hussey, Gross violation of the Wiedemann-Franz law in a quasi-one-dimensional conductor, Nat. Commun. **2**, 396 (2011).

[12] D. J. Singh, Multiband Superconductivity of Ta_4 Pd_3 Te_{16} from Te *p* States, Phys. Rev. B **90**, 144501 (2014).

[13] J. P. Perdew and A. Zunger, Self-interaction correction to density-functional approximations for many-electron systems, Phys. Rev. B **23**, 5048 (1981).

[14] P. Giannozzi, S. Baroni, N. Bonini, M. Calandra, R. Car, C. Cavazzoni, D. Ceresoli, G. L. Chiarotti, M. Cococcioni, I. Dabo, A. D. Corso, S. d. Gironcoli, S. Fabris, G. Fratesi, R. Gebauer, U. Gerstmann, C. Gougoussis, A. Kokalj, M. Lazzeri, L. Martin-Samos, N. Marzari, F. Mauri, R. Mazzarello, S. Paolini, A. Pasquarello, L. Paulatto, C. Sbraccia, S. Scandolo, G. Sclauzero, A. P. Seitsonen, A. Smogunov, P. Umari, and R. M. Wentzcovitch, QUANTUM ESPRESSO: A modular and open-source software project for quantum simulations of materials, J. Phys.: Condens. Matter **21**, 395502 (2009).

[15] A. Kokalj, XCrySDen a new program for displaying crystalline structures and electron densities, J. Mol. Graph. Mod. **17**, 176 (1999).

[16] P. M. C. Rourke and S. R. Julian, Numerical extraction of de Haas–van Alphen frequencies from calculated band energies, Comput. Phys. Commun. **183**, 324 (2012).

[17] M. Rotter, M. Tegel, D. Johrendt, I. Schellenberg, W. Hermes, and R. Pttgen, Spin-density-wave anomaly at 140 k in the ternary iron arsenide $BaFe_2As_2$, Phys. Rev. B **78**, 020503 (2008).

[18] D. Shoenberg, *Magnetic Oscillations in Metals* (Cambridge University Press, Cambridge, 1984).

[19] Q. Fan, W. H. Zhang, X. Liu, Y. J. Yan, M. Q. Ren, M. Xia, H. Y. Chen, D. F. Xu, Z. R. Ye, W. H. Jiao, G. H. Cao, B. P. Xie, T. Zhang, and D. L. Feng, Scanning tunneling microscopy study of superconductivity, magnetic vortices, and possible charge-density wave in Ta_4 Pd_3 Te_{16}, Phys. Rev. B **91**, 104506 (2015).

[20] P. A. Lee, T. M. Rice, and P. W. Anderson, Fluctuation Effects at a Peierls Transition, Phys. Rev. Lett. **31**, 462 (1973).

[21] H. Yoshiyama, Y. Takaoka, N. Suzuki, and K. Motizuki, Effects on lattice fluctuations on the charge-density-wave transition in transition-metal dichalcogenides, J. Phys. C: Sol. State Phys. **19**, 5591 (1986).

[22] G. Grüner, *Density Waves in Solids* (Perseus, Cambridge, MA, 1994).

[23] F. Flicker and J. van Wezel, Charge order from orbital dependent coupling evidenced by $NbSe_2$, Nat. Commun. **6**, 7034 (2015).

[24] W. L. McMillan, Theory of discommensurations and the commensurate-incommensurate charge-density-wave phase transition, Phys. Rev. B **14**, 1496 (1976).

[25] Y. Feng, J. van Wezel, J. Wang, F. Flicker, D. M. Silevitch, P. B. Littlewood, and T. F. Rosenbaum, Itinerant density wave instabilities at classical and quantum critical points, Nat. Phys. **11**, 865 (2015).

[26] R. M. Fleming, L. F. Schneemeyer, and D. E. Moncton, Commensurate-incommensurate transition in the charge-density-wave state of $K_{0.30}MoO_3$, Phys. Rev. B **31**, 899 (1985).

[27] E. H. da Silva Neto, R. Comin, F. He, Y. Sutarto, R. Jiang, R. L. Greene, G. A. Sawatzky, and A. Damascelli, Charge ordering in the electron-doped superconductor $Nd_{2-x}Ce_xCuO_4$, Science **347**, 282 (2015).

[28] E. M. Forgan, E. Blackburn, A. T. Holmes, A. K. R. Briffa, J. Chang, L. Bouchenoire, S. D. Brown, R. Liang, D. Bonn, W. N. Hardy, N. B. Christensen, M. V. Zimmermann, M. Hucker, and S. M. Hayden, The microscopic structure of charge

density waves in underdoped $YBa_2Cu_3O_{6.54}$ revealed by x-ray diffraction, Nat. Commun. **6**, 10064 (2015).

[29] W.-H. Jiao, Y. Liu, Y.-K. Li, X.-F. Xu, J.-K. Bao, C.-M. Feng, S. Y. Li, Z.-A. Xu, and G.-H. Cao, Multiband superconductivity in $Ta_4Pd_3Te_{16}$ with anisotropic gap structure, J. Phys.: Condens. Matter **27**, 325701 (2015).

[30] D. Chen, P. Richard, Z.-D. Song, W.-L. Zhang, S.-F. Wu, W. H. Jiao, Z. Fang, G.-H. Cao, and H. Ding, Raman scattering investigation of the quasi-one-dimensional superconductor $Ta_4Pd_3Te_{16}$, J. Phys.: Condens. Matter **27**, 495701 (2015).

[31] C. Schlenker, C. Hess, C. Le Touze, and J. Dumas, Charge density wave properties of quasi low-dimensional transition metal oxide bronzes, J. Phys. I France **6**, 2061 (1996).

[32] M. Naito and S. Tanaka, Electrical transport properties in 2H-NbS_2, -$NbSe_2$, -TaS_2 and -$TaSe_2$, J. Phys. Soc. Japan **51**, 219 (1982).

[33] F. Flicker and J. van Wezel, Charge ordering geometries in uniaxially strained $NbSe_2$, Phys. Rev. B **92**, 201103 (2015).

[34] B. Köhler, E. Rose, M. Dumm, G. Untereiner, and M. Dressel, Comprehensive transport study of anisotropy and ordering phenomena in quasi-one-dimensional $(TMTTF)_2X$ salts ($X =$ PF_6, AsF_6, SbF_6, BF_4, ClO_4, ReO_4), Phys. Rev. B **84**, 035124 (2011).

[35] J. L. Cohn, S. Moshfeghyeganeh, C. A. M. dos Santos, and J. J. Neumeier, Extreme Thermopower Anisotropy and Interchain Transport in the Quasi-One-Dimensional Metal $Li_{0.9}Mo_6O_{17}$, Phys. Rev. Lett. **112**, 186602 (2014).

[36] P. Monceau, Electronic crystals: An experimental overview, Adv. Phys. **61**, 325 (2012).

[37] A. Sinchenko, P. D. Grigoriev, P. Lejay, O. Leynaud, and P. Monceau, Anisotropy of conductivity in rare-earth tritellurides in the static and sliding states of the CDW, Physica B **460**, 21 (2015).

[38] V. Brouet, W. L. Yang, X. J. Zhou, Z. Hussain, R. G. Moore, R. He, D. H. Lu, Z. X. Shen, J. Laverock, S. B. Dugdale, N. Ru, and I. R. Fisher, Angle-resolved photoemission study of the evolution of band structure and charge density wave properties in R Te_3 ($R =$ Y, La, Ce, Sm, Gd, Tb, and Dy), Phys. Rev. B **77**, 235104 (2008).

[39] F. Flicker and J. van Wezel, One-Dimensional Quasicrystals from Incommensurate Charge Order, Phys. Rev. Lett. **115**, 236401 (2015).

[40] S. Kagoshima, T. Ishiguro, and A. Hiroyuki, X-ray scattering studies of phonon anomalies and superstructures in TTF-TCNQ, J. Phys. Soc. Japan **41**, 2061 (1976).

[41] J. Bardeen, Depinning of charge-density-waves by quantum tunneling, Phys. Scr. **T27**, 136 (1989).

[42] Z. Li, W. H. Jiao, G. H. Cao, and G. Zheng, Charge fluctuations and nodeless superconductivity in quasi-one-dimensional $Ta_4Pd_3Te_{16}$ revealed by ^{125}Te-NMR and ^{181}Ta-NQR, Phys. Rev. B **94**, 174511 (2016).

[43] H. Nishihara, K. Hayashi, M. Naito, T. Butz, A. Lerf, and S. Saibene, NQR and low-field NMR of ^{181}Ta in the low-temperature CDW state of 2H-TaS_2, Z. Naturforsch. **45**, 412 (1990).

[44] R. M. Fernandes, A. V. Chubukov, and J. Schmalian, What drives nematic order in iron-based superconductors, Nat. Phys. **10**, 97 (2014).